P3.18 **COUPLING A MOSAIC LAND SURFACE SCHEME (SIBUC) WITH A NONHYDROSTATIC ATMOSPHERIC MODEL (ARPS)**

Kazuyoshi Souma*, Kenji Tanaka, Eiichi Nakakita and Shuichi Ikebuchi Kyoto University, Kyoto, Japan

1. INTRODUCTION

Heating from land surface and intensity of local circulation can affect transport of moisture and cumulous clouds. Various researches on understanding the effect of topography to the transport of moisture and cumulous clouds (e.g. Kimura and Kuwagata (1995)) have been carried out, however, the effect of land surface conditions are still poorly understood.

In this study, an advanced land surface process model called Simple Biosphere model including Urban Canopy (SiBUC; Tanaka et al. (1998)) is coupled into a mesoscale numerical atmospheric model. The Advanced Regional Prediction System (ARPS; Xue et al. (1995)), which has been developed by the Center for Analysis and Prediction of Storms, Unversity of Oklahoma is used as the mesoscale numerical model.

During the intensified field campaign of the Lake Biwa Project 2001, well developed local circulation is observed in the Lake Biwa Basin in Japan (the location is shown in **Figure. 1**) on a typical summer sunny day (14th August 2001). This case is simulated by the original ARPS (with simple land surface model) and the ARPS coupled with the SiBUC model (ARPS-SiBUC).

The effects of urban area and subgrid scale land use to the intensity of local circulation within the Lake Biwa Basin are also discussed by the comparison of the simulated values with observed values.

In the Lake Biwa Project, surface flux data have been observed at three regular flux measurement sites, named paddy field, lake and forest sites, respectively (the locations are shown in **Figure. 1**). During the intensified field campaign of the Lake Biwa Project, radiosonde observations were carried out near the paddy field site. We can also obtain Upper air, surface observation and AMeDAS data.

2. DESCRIPTION OF THE LAND SURFACE SCHEME (LSS)

The original ARPS has a land surface scheme (LSS) based on Interactions between the Soil Biosphere and Atmosphere (ISBA; Noilhan et al., 1989) (Pleim et al., 1995). Only natural land surface areas such as forest, grassland and bare soil are considered in the LSS.

The SiBUC model has been developed by the Disaster Prevention Research Institute, Kyoto University. It uses mosaic approach, in which the grid averaged surface fluxes are obtained by averaging the surface fluxes over each land-use weighted by its fractional area. In the SiBUC model, the surface of each grid area is divided into three land use categories and the surface fluxes are calculated by three sub-models: green area model, urban area model and water body model. For the green area model, the Simple Biosphere model (SiB; Sellers et al., 1986) was adopted and some modifications from the original SiB (such as simplification and installing paddy field model) have been implemented.

* *Corresponding author address:*
Kazuyoshi Souma,
Graduate School of Engineering, Kyoto University, Sakyo, Kyoto, 606-8501, Japan;
e-mail: souma@wrcs.dpri.kyoto-u.ac.jp

3. EXPERIMENTAL DESIGN

3.1 *Configuration of atmospheric model*

Two calculations are performed for 12 hours from 03:00JST on 14th August during the intensified observation period of the Lake Biwa Project. The first calculation is performed by the original ARPS coupled with the ISBA model and named Case1. The other calculation is performed by the ARPS coupled with the SiBUC model and named Case2. The model configuration of the ARPS is shown in **Table. 2** and its application domain is shown in **Figure. 1**. Three domains named step1, step2 and step3, respectively, are set. The simulated values in the step3 domain will be discussed.

The Grid Point Value (GPV) data of the Regional Spectral Model (RSM, a hydrostatic model used for operational forecast in Japan), which have about 40km of resolution and 3-hour interval are used as initial and boundary conditions for simulation in the step1 domain. The results of step1 is nested-down to step2 and step3 (one-way nesting). Upper air, surface observation and AMeDAS data are assimilated to produce initial field by the ARPS Data Assimilation System (ADAS; Xue et al. (1995)). The location of observation point is also shown in **Figure. 1**.

3.2 *Configuration of LSS*

The fractional areas of land uses (urban area, water body and 10 category of green area) and canopy frac-

Table. 1 The name of each simulation

	The model used in each simulation
Case1	the ARPS coupled with the ISBA model (original)
Case2	the ARPS coupled with the SiBUC model (ARPS-SiBUC)

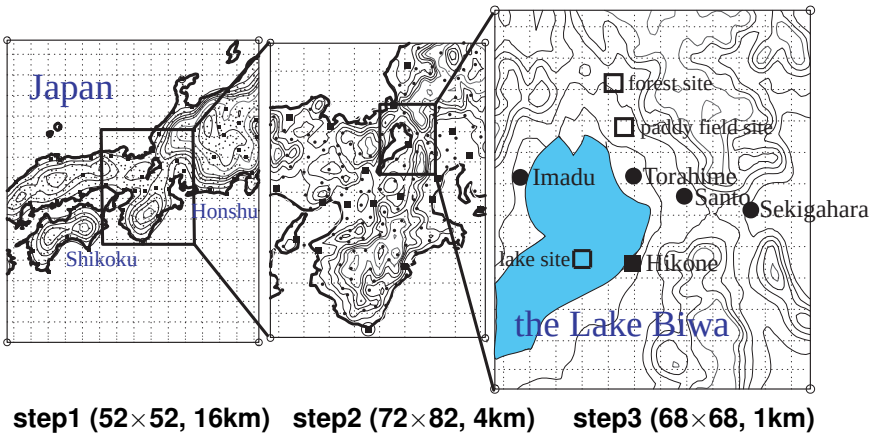

Figure. 1 Model domains and location of meteorological stations（● AMeDAS, ■ SDP (surface observation) , ○ upper air observation, □ Regular flux measurement sites of the Lake Biwa Project）

Table. 2 Model configuration

Dynamic Framework	Nonhydrostatic and fully compressible(3-D)
Coordinate System	Vertically-stretched terrain-following grid(43 layer) (Lowest level is 40m AGL. Model top is 16 km MSL) Rayleigh damping is applied to the upper 1/3 of the domain
Solution Technique	Mode-split with vertically-implicit option
Divergence Damping	divergence-damped Acoustic calculation
Top & Bottom Boundary Conditions	rigid wall
Lateral Boundary Conditions	externally-forced boundary conditions GPV from Regional Spectral Model(JMA)
Computational Mixing	4th-order
Advection	4th-order,simple positive definite scheme for water and TKE
Cloud Microphysics	3 ice-phase Microphysics(Lin-Tao)
Cumulus Parameterization	Kain-Fritsch(only for step1)
Subgrid Scale Turbulence	1.5-order turbulent kinetic energy formulation
Surface Layer	bulk aerodynamic drag laws with stability-dependent
Soil Model	1-layer Soil and Surface Energy Balance Model(ISBA) 11 Soil Categories, 13 Vegetation Categories
Longwave and Shortwave Radiation	Atmospheric Radiative Transfer
time step	step1:12sec, step2:5sec and step3:5sec, respectively

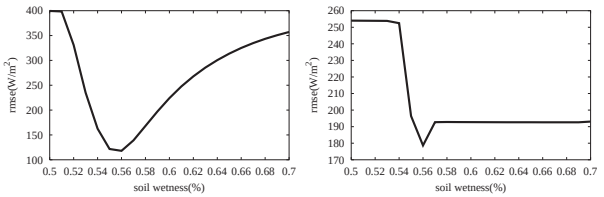

Figure. 2 Sum of the RMSE of sensible and latent heat flux on 24th August in offline simulations at the forest site

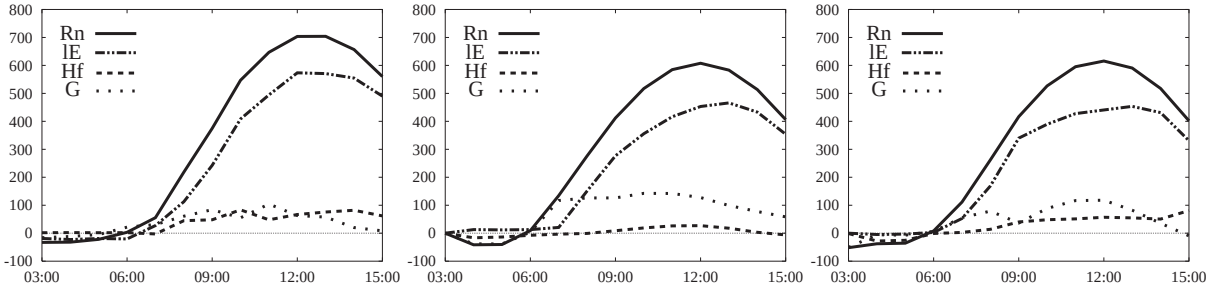

Figure. 3 Energy budget at the paddy field site（W/m^2）（Rn:net radiation, lE:latent heat flux, Hf:sensible heat flux, G:heat storage）

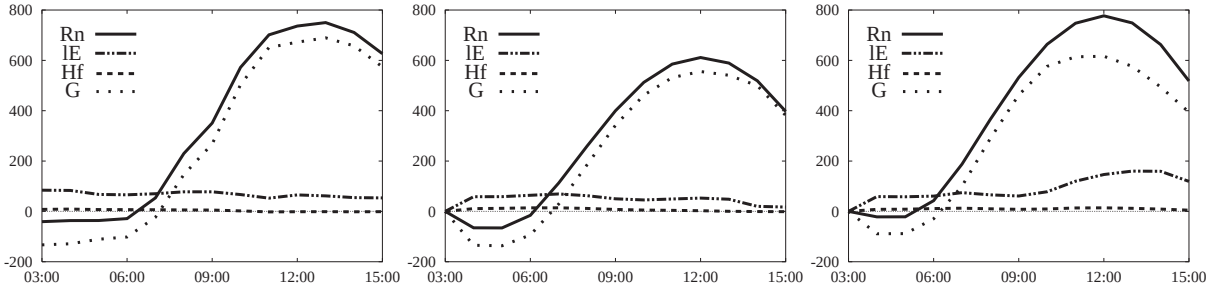

Figure. 4 Energy budget at the lake site（W/m^2）（Rn:net radiation, lE:latent heat flux, Hf:sensible heat flux, G:heat storage）

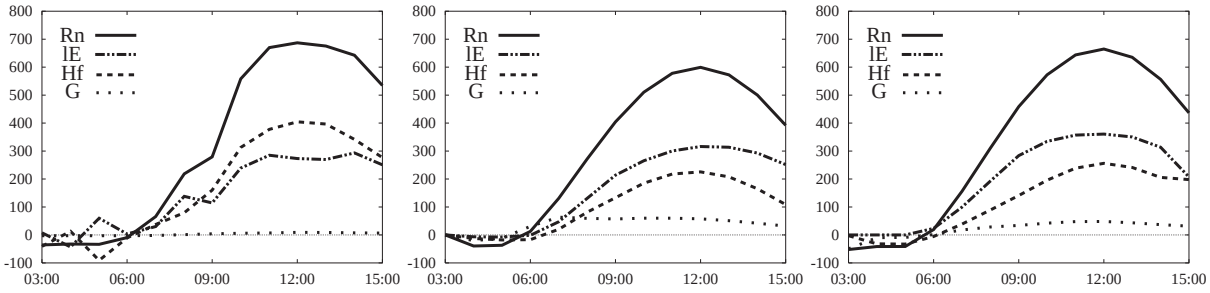

Figure. 5 Energy budget at the forest site（W/m^2）（Rn:net radiation, lE:latent heat flux, Hf:sensible heat flux, G:heat storage）: Reference flux data was obserbed on 24th August

tion within each land use are assigned to each grid. In this study, KS-202 data (with about 100m resolution and 15 land use categories) are reclassified into the land use fraction dataset with seven categories (paddy, farmland, grassland, mixed forest, bare soil, urban area, and water) and the reclassified dataset is used to calculate the fractional areas.

NDVI (Normalized Difference Vegetation Index) of Global AVHRR 10-day composite data (about 1km resolution) made by USGS (U.S. Geological Survey) are used to estimate the LAI (Leaf Area Index) in green areas.

As for soil type, a global digital soil map from FAO (Food and Agricultural Organization of the United Nations), which has about 10km resolution and more than 1000 categories is used. According to the detailed soil texture information for each soil type, this dataset is reclassified into 11 categories, such as sand and loamy sand.

Initial land-surface temperature is calculated from near-surface atmospheric temperature. As for initial sea-surface temperature, monthly averaged dataset of NOAA/ NASA AVHRR Oceans Pathfinder SST is used, which has about 9km resolution. As for initial lake-surface temperature of the Lake Biwa, the monthly averaged observation data at the lake site are used.

In order to define initial soil moisture, some offline simulations are carried out at the forest site. In the offline simulations with the ISBA and SiBUC models, the initial soil moisture is changed from 0.5 to 0.7 in wetness (shown in **Figure. 2**). Initial soil moisture is optimized so as to minimize the sum of RMSE of sensible and latent heat flux. Finally, initial soil moisture is defined as 0.56 in wetness.

As for the grids classified as cultivation in the ISBA model, initial soil moisture is set to 1.0 in wetness, because basically all crops are identified as paddy field in the step3 domain.

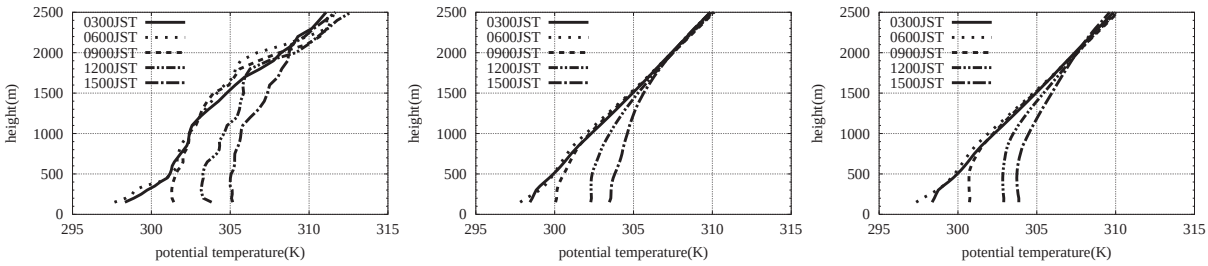

Figure. 6 Vertical profiles of potential temperature at different time on 14th August near the paddy field site

4. RESULTS AND DISSCUSSION

4.1 *Surface flux*

Figure. 3, **Figure. 4** and **Figure. 5** show each term of land surface energy budget equation ($R_n = Hf + lE + G$) at the paddy field, lake and forest sites (shown in **Figure. 1**). Observed data of 24th August are used as reference data at forest because observed data could not be obtained for 14th August. Observed flux data are calculated by Bowen ration method for paddy and forest, and by stability dependent Bulk method for lake, respectively.

Figure. 3 shows that the feature of observed surface flux at paddy field, which has a large rate of latent heat flux compared to net radiation, is simulated very well by both Case1 and Case2. Although the SiBUC model is composed by a paddy field model, difference between the results of surface flux at paddy field simulated by Case1 and Case2 does not seem to be much evident.

Figure. 4 shows that net radiation simulated by Case1 is less than the observation. Diurnal variation of latent and sensible heat flux is simulated well by Case1 and Case2. This difference in net radiation does not seem to affect much on the local circulation.

Figure. 5 shows that simulated latent heat flux is larger and simulated sensible heat flux is smaller than that of the reference values in both simulations of Case1 and Case2. The simulated surface flux is a little different from the reference values, however, the simulated flux by Case1 and Case2 are not very different from each other.

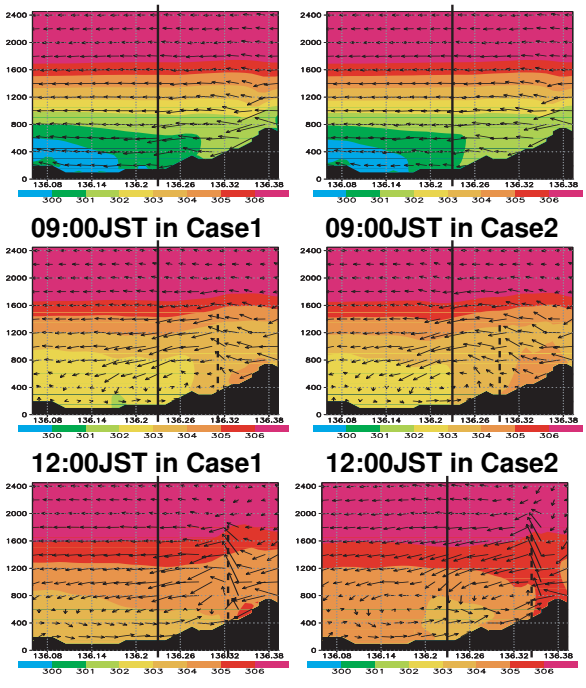

Figure. 7 East-west vertical cross section of potential temperature(K) and wind vector at the paddy field site. The solide lines indicate the position of vertical profile in **Figure. 6**. The dashed lines represent the positions of the lake breeze front

4.2 *Local circulation within the Lake Biwa Basin*

(1) Vertical profiles of potential temperature

The left figure of **Figure. 6** shows vertical profiles of potential temperature observed by radiosonde near the paddy field site. In this figure, two mixed layers can be seen at 12:00JST. First one is defined from surface to about 700m, where the profile of potential temperature shows almost neutral, and the other layer is defined from 700m to about 1800m, where potential temperature increases and vertical gradient becomes smaller than 09:00JST. According to Kimura and Kuwagata (1995), the lower mixed layer is caused by turbulent diffusion, whereas upper mixed layer is caused by heat transport with local circulation. An extended mixed layer, defined from surface to about 2000m, can be also seen at 15:00JST.

Figure. 6 shows that both Case1 and Case2 can simulate the feature found in observed vertical profiles of potential temperature qualitatively. The height of the mixed layer in Case1 and Case2 are about 1600m and 1800m, respectively, whereas the observed value is about 2000m. The height of the mixed layer in Case2 is better than Case1. This suggests that the amount of heat transportation from the eastern mountainous part to the valley bottom by the local circulation in Case2 is more than that in Case1. This may be explained that heat from land surface in Case2 is stronger than Case1, as described later. East-west vertical cross section of potential temperature is shown in **Figure. 7**. It can be seen that the potential temperature in Case2

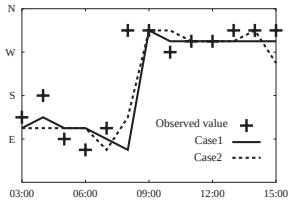

Figure. 8 Wind direction at Hikone, on the east shore of the Lake Biwa (shown in **Figure. 1**)

Figure. 9 Schematic image of the local circulation within the Lake Biwa Basin according to observed data

is higher than Case1.

(2) Wind direction on the east shore of the Lake Biwa

The wind direction data observed by AMeDAS show that the lake breeze was well developed on the east shore of the Lake Biwa. However, the up-valley wind was not developed in the eastern mountainous part of the Lake Biwa Basin on 14th August. During the morning period, the in-situ data, which is shown in **Figure. 8**, show that wind direction on the east shore of the Lake Biwa was east in general. In the afternoon period, the lake breeze developed and wind direction was changed from east to west on the east shore of the Lake Biwa as shown in **Figure. 9**.

It is shown in **Figure. 7** that the development of the lake breeze and passing of the lake breeze front over the east shore of the Lake Biwa are simulated well by both Case1 and Case2.

The change of wind direction on the east shore of the Lake Biwa simulated by both Case1 and Case2 are also shown in **Figure. 8**. Although the time when wind direction change from east to west presents an one-hour delay for both Case1 and Case2, it could be seen that Case1 and Case2 can qualitatively simulate the changes of wind direction.

(3) Comparison of simulation with surface observation data

Near surface wind speed and temperature are compared with observation at 8 points in the right panel of **Figure. 1**, and root mean square error is listed in **Table. 3**. We can see that the accuracy of temperature in Case2 is better than that in Case1. This may be explained as near surface temperature on the east shore of the Lake Biwa is underestimated in Case1 (shown

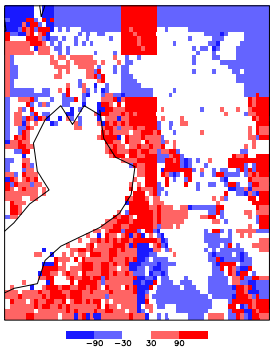

Figure. 10 Difference of sensible heat flux (W/m^2: Case2 - Case1) at 12:00JST on 14th August

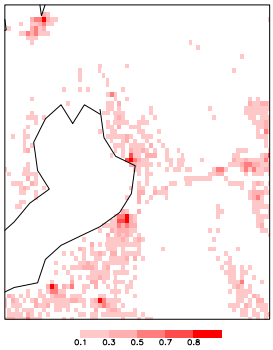

Figure. 11 Fraction of urban area in each grid

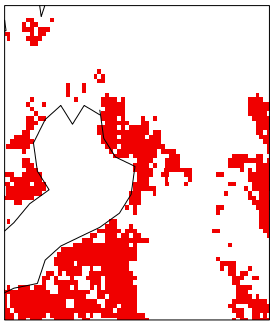

Figure. 12 The grids in which land uses are classified as cultivation in the ISBA model

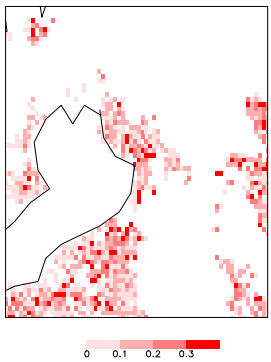

Figure. 13 The fractions of urban area in the grids shown in **Figure. 12**

in **Figure. 7**) and the underestimation is decreased by stronger heat from land surface in Case2 than Case1.

(4) Heat from land surface

Figure. 10 shows the difference between the sensible heat flux (i.e. heat from land surface) in Case2 and Case1. Although the coarse resolution of soil type data causes a little unreal horizontal distribution of sensible heat flux in the ISBA model, it can be seen that difference of the sensible heat flux is not seen on the lake and in the mountainous area (mostly forest). This agree with the discussion about **Figure. 4** and **Figure. 5**. On the other hand, sensible heat flux in Case2 is lager on the east shore of the Lake Biwa than that in Case1.

Figure. 11 shows the fraction of urban area in each grid. The grids in which the ratio of urban area is large can be seen on the east shore of the Lake Biwa.

Figure. 12 shows the grids in which the fractions of paddy field are the largest and land uses are classified as cultivation in the ISBA model. **Figure. 13** shows the fractions of urban area in such grids. It can be seen that fractions of urban area is not small in such grids.

Figure. 3 shows that difference between the results of surface flux at paddy field simulated by Case1 and

Case2 does not seem to be much evident. Therefore, the increase in sensible heat flux results from increase of heat from land surface by urban canopy model and subgrid scale land use (especially in small urban area) expressed by the mosaic scheme in the SiBUC model.

The stronger turbulent diffusion is caused by the stronger sensible heat flux on the east shore of the Lake Biwa in Case2 than Case1. The stronger heat transport by local circulation is caused by more difference of sensible heat flux between the Lake Biwa and the east shore of the Lake Biwa in Case2 than Case1. The higher near surface temperature on the east shore of the Lake Biwa (shown in **Figure. 7**) is caused by the stronger turbulent diffusion and the stronger heat transport by local circulation in Case2 than Case1.

Therefore, it is indicated that smaller RMSE of near surface temperature (i.e. higher near surface temperature on the east shore of the Lake Biwa) in Case2 results from the larger sensible heat flux caused by urban canopy model and subgrid scale land use expressed by the mosaic scheme in the SiBUC model.

Table. 3 Results of root mean square error of near–surface wind speed and temperature between simulation and observed data at 8 points, which are shown in **Figure. 1**

	Case1	Case2
Wind speed(m/s)	1.0	0.9
Air temperature(K)	1.85	1.47

5. CONCLUTIONS

In this study, an advanced land surface process model SiBUC has been coupled into a mesoscale numerical atmospheric model ARPS.

Through the comparison of the simulated atmospheric fields with surface observation data and radiosonde data, it turns out that mosaic approach and urban canopy model of SiBUC can improve the development of local circulation and accuracy of near surface air temperature.

Acknowledgements

In this study, the Advanced Regional Prediction System, which has been developed by the Center for Analysis and Prediction of Storms, Unversity of Oklahoma is used. Authors are grateful to the Dr. Nobuhiro Ebisu (Ehime University) for observation at the forest site.

References

[1] Kimura,F. and kuwagata,T., 1995 : Horizontal heat fluxes over complex terrain computed using a simple mixed-layer model and a numerical model, J. Appl. Meteor., pp.549-558

[2] Noilhan,J. and Planton,S., 1989 : A simple parameterization of land surface processes for meteorological models, Mon. Wea. Rev., 117, pp.536-549

[3] Pleim,J.E. and Xiu,A., 1995 : Development and Testing of a Surface Flux and Planetary Boundary Layer for Application in Mesoscale Models, J. Appl. Meteor., 34, pp.16-32

[4] Sellers,P.J., Mintz,Y., Sud,Y.C. and Dalcher,A., 1986 : A simple biosphere model(SiB) for use within general circulation models, J. Atmos. Sci., 43,505-531

[5] Tanaka, K., Nakakita, E. and Ikebuchi, S., 1998:Land-surface Parameterization in the Lake Biwa Project, Annual Journal of Hydraulic Engineering, JSCE, 42, pp.79-84 (in Japanses)

[6] Xue,M., Droegemeier,K.K., Wong,V., Shapiro,A. and Brewster,K., 1995:Advanced Regional Prediction System(ARPS) Version 4.0 User's Guide